Progress in CryoEM analysis of human PreP

Recombinant human PreP was expressed in *E. coli* and purified using Ni-NTA, Source Q anion exchange, and S200 columns according to King et al Structure 22:996-10017, 2014. The purified human PreP behaves as a monomer based on size exclusion column, a finding consistent with previous SAXS analysis. Human PreP has 16 cysteine residues, which contributes to its high sensitivity to oxidative inactivation. PreP is a zinc metalloprotease and the presence of EDTA can strip the catalytic zinc ion, rendering PreP inactive. We thus vary the reducing agents (beta-mercaptoethanol, dithiothreitol (DTT), or Tris(2-carboxyethyl)phosphine (TCEP)) and metal chelator (EDTA) in addition to the conventional conditions, i.e., NaCl (50-300 mM), buffers (Tris, Hepes), the type of grid (Au, Cu), and blotting time controlled by vitribot for the grid preparation. By optimizing these variables using the 200 KV Talos at the University of Chicago, we have found conditions that are optimal to image the monomeric PreP particles in the PreP alone condition using a 200 mesh Cu grid.

Previous approval by the review committee allowed us to visit NCCAT for two-day on-site data collection from October 4-6. In this period, we obtained ~3,300 micrographs containing ~650,000 particles. Using Relion 3.0 and Cryosparc, we have obtained good 2D class averages (Figure 1A). To avoid model bias, we used the structure of plant PreP as a model, instead of the human PreP structure. After significant effort in our data analysis, a satisfactory 3D classification emerged to reveal two major classes of PreP structures that are distinct from the previously published, closed state, crystal structure of PreP (Figure 1 and 2). A 5.1 angstrom structure of open state PreP was reconstructed from 45,292 particles while a 4.5 angstrom structure of a partial open state PreP was reconstructed from 34,404 particles.

Figure 1 CryoEM analysis of PreP open state structure. (A) 2D classification. (B) PreP open state model (ribbon) and Coulomb potential density map. (C) Comparison of PreP open state structure with PreP closed state. (D) FSC plot of PreP open state structure, indicating 5.1 angstrom resolution. (E) Angular distribution plot depicting the severe orientation bias. (F) ResLog plot for the resolution estimation when the additional data is added.

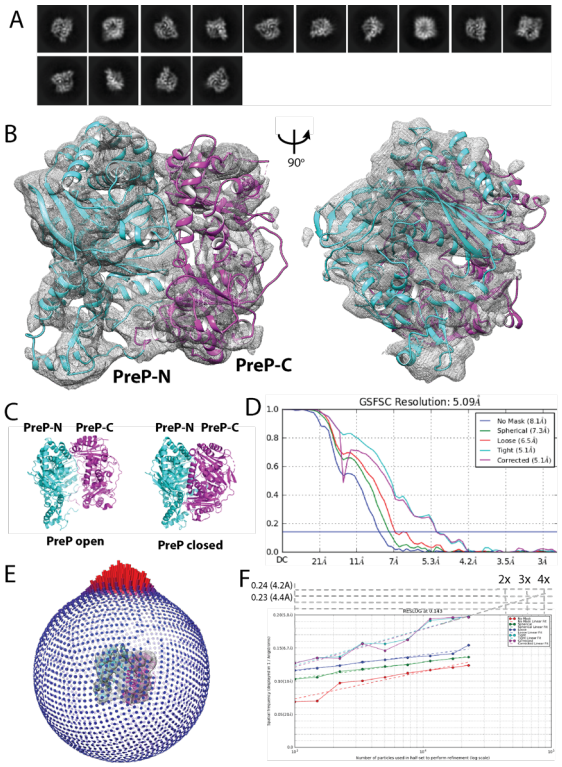

Figure 2 CryoEM analysis of PreP partial open state. (A) PreP partial open state (ribbon) and Coulomb potential density map. (B) Comparison of PreP partial open state (cyan and magenta) with PreP closed state (pale cyan). (C) FSC plot of PreP partial open state structure, indicating 4.5 angstrom resolution. (D) Angular distribution plot. (F) ResLog plot for the estimated resolution improvement with additional data.

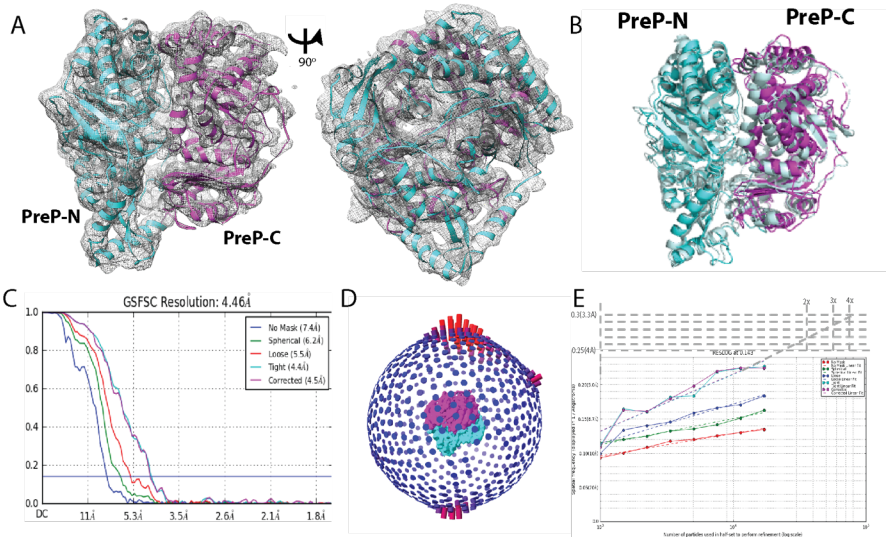

PreP has ~50 kDa N and C domains (PreP-N and PreP-C, respectively) connected by an alpha-helical hair-pin (Figure 1C). Compared with the PreP closed structure, the open-state PreP structure reveals a large-scale pivot motion between PreP-N and PreP-C (Figure 1C, 1D). However, detailed analysis of this molecular motion is hampered by poor map quality stemming from severe orientation bias (Figure 1E). We estimate that 3 times additional data with the tilted series should improve the resolution up to 4.3 angstrom and better density map for the modeling (Figure 1F).

The partial open PreP structure represents a ~7 angstrom opening between PreP-N and PreP-C in comparison with the crystal structure of PreP closed state (Figure 2A-C). In this case, we observed a mild orientation bias. We estimate that 3 times additional data should push the resolution of this structure beyond 3.5 angstrom.

In addition to the expected open state structures of PreP from our 3D classification, we also obtained a PreP structure that has an intact PreP-N and denatured PreP-C despite the fact that purified PreP behaved as a single uniform species in size exclusion column and greater than 95% PreP is intact based on SDS-PAGE (Figure 3). This structure prefers to adopt an orientation such that the presumably denatured PreP-C faces the incoming electron beam while PreP-N is opposite to that. Thus, it is reasonable to assume that this structure is derived from unfavorable interactions between PreP-C and the air-water interface, which is known to cause the denaturation of protein. This also explains the significant difficulty that we had in our 3D classification for generating an interpretable density map and the lower number of usable particles for the two open state PreP structures. We have attempted to use amine-to-amine crosslinker, DSS to rigidify the PreP-C domain so that PreP can withstand the denaturation by the air-water interface. However, such treatment has worsened the denaturation problem. The addition of additives, e.g., detergent or organic solvent has also failed to modify the vitrified ice and/or change the surface properties better favor intact PreP particles. In fact, these efforts have mostly resulted in conditions where PreP is excluded from the grid holes. We will continue to explore the conditions that can favor intact PreP in the vitrified ice, yet is our belief, as detailed above, that the primary cause of PreP-C denaturation is prolonged exposure to the air-water interface during grid preparation. We anticipate that the use of spotiton in grid preparation will vastly decrease the amount of PreP-C denaturation. The commensurate increase in analyzable intact PreP particles should also reduce the amount of data collection necessary to reach our desired resolution, ultimately saving both time and money.

Figure 3 Partially denatured PreP structure. (A) The size exclusion profile of purified PreP and SDS-PAGE and Coomassie blue staining of PreP peak fraction. (B) The partially denatured PreP structure with PreP-N in ribbon representation and Coulomb potential density map in grey.